UNIVERSITY OF BIRMINGHAM
University of Birmingham Research at Birmingham

Influence of magnetic field upon electrode kinetics and ionic transport

Chen, Yongxiu; Alder, James; Song, Tengfei; Chen, Lin; Sheridan, Richard; Davenport, Alison; Kendrick, Emma

DOI:
10.1016/j.jpowsour.2024.234323

License:
Creative Commons: Attribution (CC BY)

Document Version
Publisher's PDF, also known as Version of record

Citation for published version (Harvard):
Chen, Y, Alder, J, Song, T, Chen, L, Sheridan, R, Davenport, A & Kendrick, E 2024, 'Influence of magnetic field upon electrode kinetics and ionic transport', *Journal of Power Sources*, vol. 602, 234323. https://doi.org/10.1016/j.jpowsour.2024.234323

Link to publication on Research at Birmingham portal

General rights
Unless a licence is specified above, all rights (including copyright and moral rights) in this document are retained by the authors and/or the copyright holders. The express permission of the copyright holder must be obtained for any use of this material other than for purposes permitted by law.

•Users may freely distribute the URL that is used to identify this publication.
•Users may download and/or print one copy of the publication from the University of Birmingham research portal for the purpose of private study or non-commercial research.
•User may use extracts from the document in line with the concept of 'fair dealing' under the Copyright, Designs and Patents Act 1988 (?)
•Users may not further distribute the material nor use it for the purposes of commercial gain.

Where a licence is displayed above, please note the terms and conditions of the licence govern your use of this document.

When citing, please reference the published version.

Take down policy
While the University of Birmingham exercises care and attention in making items available there are rare occasions when an item has been uploaded in error or has been deemed to be commercially or otherwise sensitive.

If you believe that this is the case for this document, please contact UBIRA@lists.bham.ac.uk providing details and we will remove access to the work immediately and investigate.

Download date: 04. May. 2024

Journal of Power Sources 602 (2024) 234323

Contents lists available at ScienceDirect

Journal of Power Sources

journal homepage: www.elsevier.com/locate/jpowsour

Influence of magnetic field upon electrode kinetics and ionic transport

Yongxiu Chen [a,b,*], James Alder [a], Tengfei Song [a], Lin Chen [a], Richard Sheridan [a], Alison Davenport [a], Emma Kendrick [a,b,**]

[a] School of Metallurgy and Materials, University of Birmingham, Edgbaston, Birmingham, BT15 2TT, UK
[b] The Faraday Institution, Quad One, Becquerel Avenue, Harwell Campus, Didcot, OX11 0RA, UK

HIGHLIGHTS

- Magnetic spacer design for improving cell rate performance in commercialization.
- Magnetic application to address short circuits in lithium/sodium-ion batteries.
- Magnetic effect of increasing reaction kinetics at the ferromagnetic cathode.
- The enhanced diffusion at the rate-limiting graphite anode from the MHD effect.
- Transferable to other cell chemistries for high-rate and long-life cell design.

GRAPHICAL ABSTRACT

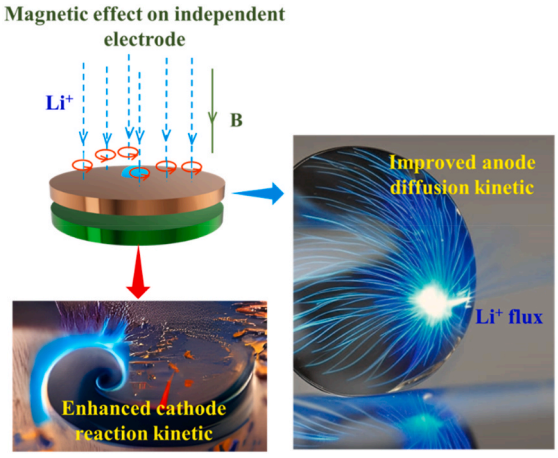

ARTICLE INFO

Keywords:
Lithium/sodium-ion batteries
Internal magnetic field
Magnetohydrodynamics
Enhanced kinetics
Dendrite inhibition
Electrochemical performance

ABSTRACT

Performance properties in lithium-ion, sodium-ion, and zero excess metal batteries are currently limited by the sluggish ion diffusion and inhomogeneity of the transport ion flux, resulting in poor formation, low rates, and short cycle lives. In this work, a magnetic field is applied to the cell by the incorporation of a NdFeB magnetic spacer, and the effect upon the kinetics and transport properties at each electrode is studied using galvanic charge and discharge, electrochemical impedance spectroscopy, and intermittent titration techniques. Stabilization of the anode-free or zero excess sodium and lithium metal cells is achieved during formation, and upon cycling. Reduced cell overpotential is observed with resulting higher areal capacities, with improved ionic diffusion through the electrode. Upon cycling metallic dendritic structures are suppressed due to the inhomogeneity of ion flux, and the likely competing kinetics of plating at a metallic tip and the surrounding surface. At the NMC electrode, improved kinetics are observed with lower charge-transfer resistance (Rct) due to the reshaped and aligned domain in the ferromagnetic Ni of NMC cathode. Pulsed current methods further confirm enhanced cationic diffusion in the anode graphite materials, particularly at high mass loading of 4 mA h

* Corresponding author. School of Metallurgy and Materials, University of Birmingham, Edgbaston, Birmingham, BT15 2TT, UK.
** Corresponding author. School of Metallurgy and Materials, University of Birmingham, Edgbaston, Birmingham, BT15 2TT, UK.
E-mail addresses: y.chen.17@bham.ac.uk (Y. Chen), emma.kendrick@bham.ac.uk (E. Kendrick).

https://doi.org/10.1016/j.jpowsour.2024.234323
Received 2 January 2024; Received in revised form 17 February 2024; Accepted 6 March 2024
Available online 15 March 2024
0378-7753/Crown Copyright © 2024 Published by Elsevier B.V. This is an open access article under the CC BY license (http://creativecommons.org/licenses/by/4.0/).

cm^{-2} and high C rates. Consequently, the combination of enhanced reaction kinetics on the ferromagnetic cathode and improved diffusion kinetics in the porous anode leads to excellent full-cell performance compared to control groups. This study highlights the potential of magnetic fields in enhancing diffusion and reaction kinetics for rechargeable batteries (Li, Na, K, Mg, etc.), and may provide routes for extending cycle life, reconditioning cells, and improving formation protocols.

1. Introduction

The ever-increasing demand for energy requires battery technologies with both high power, energy density and long life [1,2]. This can be achieved through careful optimisation of the cell chemistries, such as lithium or sodium ion, their components and manufacturing processes [3,4]. Power energy, and cycle life are often decoupled and cells are optimized for a specific property. Methods to improve the rate of high-energy density batteries, and their cycle-life are required [5–8]. Further improvements in energy density can be achieved with lithium or sodium metal batteries (LMB/SMB) which have high theoretical negative electrode capacities (3860 mA h g^{-1} for LMB and 1166 mA h g^{-1} for SMB) [9–11] However, challenges in the mass transport of ions, the rate of electron transfer, and many degradation mechanisms need to be solved [12–14]. One key failure mechanisms for both metal-ion and metal systems is dendritic growth at the surface of the anode due to the repeated stripping and plating, which can lead to short-circuiting the cell, Coulombic inefficiencies from constant SEI growth and capacity loss [15–19].

Inhibition of metal dendrites has been partially achieved through mechanical blocking methods such as robust SEI layer or separator [20,21], solid-state electrolyte [22], also ionic mass transport methods such as pulse charging style [23,24], external physical field [25–28], electrode design [29,30], and chemical methods to modify the metallic deposition behaviour such as electrolyte additives [31], or functionalized negative electrodes (doping, core-shell methodology, etc) [32]. Although progress has been achieved, these approaches are reliant upon chemical modification of the surfaces and interfaces with little control of these reactions. Typically, the initial interface formation occurs in the first few cycles and is controlled through current, voltage and temperature continuous rearrangements of these interfaces occur during cycling, this determines the capacity and life-time of the cells [33,34]. However, further growth occurs over time and during cycling leading to cell degradation. Previous research demonstrates that dendrite formation can be inhibited through control of metal ion diffusivity in the electrolyte, through a process called magneto hydrodynamic forces or effects (MHD) [35,36]. Magnetic fields have been widely investigated in electrodeposition for metal ions, which involve magnetohydrodynamics (MHD) effects. When a ferromagnetic ion (Cu^{2+}, Ag^{+}, Li^{+}, etc.) is moving in a perpendicular magnetic field with flux density B, a Lorentz Force ($F_L = I \times B$, where I is the current density) is exerted on it. This MHD effect induces liquid convection in the solution and therefore controls the morphology and deposition of the plating ion.

Previous research shows external magnetic fields applied to a lithium-ion and lithium metal batteries and a subsequent reduction in dendritic plating [26–28]. This is reported to be due to diffusion enhancement of Li^{+} via as shown by computational simulation [26]. It is necessary to explore how magnets can be incorporated into electronic applications effectively, without adding weight which reduces the overall energy density. However, this is the subject of further work. In this study, we incorporate a permanent magnet into a coin cell to investigate the effect upon the transport properties of the individual electrodes and the cell and investigate the effect upon different cell chemistries; lithium and sodium ion (low and high coat weight electrodes) and zero excess metal (anode free) lithium and sodium batteries. In all cases, we observe greater reproducibility of the capacities during the first cycles, reduced dendrite and metal plating during cycling enabling longer cycle life, and improved rate from faster diffusivity of the transport ions in the electrolyte combined with faster electron kinetics at the cathode surfaces.

2. Experimental section

2.1. Lithium-ion battery

For lithium-ion batteries, single-layer cells supplied by AMTE Power (NMC622//graphite) were adopted. The cathode (NMC622) had a high areal capacity of 4 mA h cm^{-2}, and the graphite anode had a capacity excess of 10% with a value of 4.4 mA h cm^{-2}. Detailed information regarding the components, mass ratio, separator, and electrolyte can be found in our previous research [37]. The NdFeB spacer used in the study was purchased with the same diameter (1.6 mm) and thickness (1 mm) as the normal steel spacer, the maximal magnetic strength around the magnetic disk is about 35 mT).

2.2. Sodium-ion battery (NMST//HC)

The $NaNi_{1/2}$ $Mn_{1/4}$ $Ti_{1/8}$ $Sn_{1/8}$ O_2(NMST) was synthesized by solid-state reaction methodology. The resulting cathode exhibited an areal capacity of 1 mA h cm^{-2}. The hard carbon used in the study was purchased from Kuraray, and the well-prepared electrode had an areal capacity of 1.1 mA h cm^{-2}. The Propylene (PP) (2325, Celgard) and glass fiber microfilter (GF/A, Whatman) were used as separators both in half and full cells. Sodium hexafluorophosphate ($NaPF_6$) electrolyte was used with the ratio ($NaPF_6$: EC/DEC = 1:1 vol%) (Fluorochem Ltd, UK).

Cell fabrication: Half-cell electrodes were assembled by Swaglok™ cells which are composed of the electrode (12 mm), Celgard 2325-GF/A combined separator (12.8 mm), and sodium foil (12 mm). Full-cell was fabricated using Swaglocks which consisted of the cathode (12 mm), anode (12 mm), and the combined separator (12.8 mm). $NaPF_6$ electrolytes in all half/full cells were used at 60 μL.

2.3. Physical analysis

Scanning electron microscopy (SEM) was used to explore the morphology of Cu, graphite, Al, and Hard carbon after cell tests. The procedures are as followings: the coin cells were disassembled and washed with DMC in the glove box for 1 h and dry for 6 h under Argon at room temperature (25 °C). Then, the morphology at the anode was obtained on a field emission scanning electron microscope (JSM 7401 F, Japan) operated at 5 kV and the probe current is 8.

2.4. Electrochemical analysis

Formation cycles were initially performed before any tests were conducted. Two formation cycles at C/20 C C-CV (C/50 current cut-off limit) charge and C/20 discharge were carried out with the following voltage limits to form stable SEI layers: (1) NMC622//graphite systems: 4.3 to 3.0 V vs Li/Li^{+}, and 4.2 to 2.5 V for full cells. (2) NMST//HC system: NMMT//Al: 4.3 to 2.0 V vs Na/Na^{+}, and 4.2 to 1.0 V for full cells.

Cycling performance for NMC622//Cu and NMC622//graphite was performed *C*C-CV charge (constant voltage at 4.2 V for current cut-off until C/50) and discharge to 2.5 V with the current density of 0.5 and 2 mA cm^{-2}. Cycling performance for NMST//HC was performed *C*C-CV charge (C/50 current limit) and C/5 discharge to 1.0 V to compare the

electrochemical performance of sodium-ion batteries with/without the internal magnetic spacer.

3. Results and discussion

A hard magnetic spacer (NdFeB) was used to replace the normal steel spacer in the coin-cell type battery. This replacement allowed for the generation of an internal magnetic field, as shown in Fig. 1. Both half-cell and full-cell configurations were investigated for lithium-ion and sodium-ion batteries to understand the magnetic effect on the cathode and anode in full cells.

3.1. Stabilization of anode-free lithium metal and reduction of overpotential

During the charging process, dendritic structures tend to form at the anode, leading to increased cell overpotential and potential cell failure. Copper current collectors have been shown to exhibit lithium-phobic properties and are prone to form dendrites even at low charging rates [38]. Therefore, anode-free lithium (NMC622//Cu) and sodium (NMST//Al) coin cells were utilized to investigate the effectiveness of the internal magnetic field (see Fig. S1).

The coin cells underwent two formation cycles at a charging rate of C/20, with the control group denoted as “C" and the magnetic group denoted as “M". A comparison between the control and magnetic groups is presented in Fig. 2. Poor reproducibility of the formation cycle in cells which contain no magnetic is observed with only C4 reaching the full capacity during the formation. All other cells (C1–C3) show dendrite growth and soft shorts occurring (Fig. 2a). All four cells which contain a magnet show repeatable formation capacities with no short circuits occurring from dendrite growth. Although C4 shows similar capacities to the magnetic group (Fig. 2b). It is clear that the deposition and morphology of metal upon the surface with a magnetic field are better controlled.

Furthermore, the overpotential of the anode-free lithium coin cells (NMC622) during the 1st and 2nd formation cycles was compared in Fig. 2c– d. The voltage profile in the control case exhibited higher values than the magnetic case during the charging process (Fig. 2c). This higher overpotential (voltage profiles) in the control group results from the limited diffusion and reaction kinetics at the electrode. In contrast, the internal magnetic field induced micro Li^+ motions through the magnetohydrodynamics (MHD) effect, therefore enhancing diffusion along the anode surface. This transport enhancement reduced the diffusion overpotential and contributed to higher attained areal capacities. A similar phenomenon was observed during the discharge process, where the magnetic case showed reduced overpotential and higher delivered voltage/capacity (Fig. 2d). Similar findings were also observed in the 2nd formation cycle, as demonstrated in Fig. S2. This methodology was extended and confirmed in sodium-free anode cells (NMST//Al), as shown in Fig. S3. The reduced overpotential and increased capacities observed in magnetic sodium-ion batteries during the formation cycles (C/20 × 2 cycles) further support that the internal magnetic field enhances metal ion diffusion kinetics and reduces cell overpotential.

3.2. Dendrite-free LIBs and SIBs from the internal magnetic field

The reduction of cell overpotential due to the internal magnetic field indicates enhanced mass transport. To investigate the magnetic effect on the morphology of deposited Li and Na, scanning electron microscope (SEM) physical characterizations were conducted on the negative electrodes of NMC622//Cu and NMST///Al, respectively, to reveal the deposited Li and Na morphology.

Fig. S4 compared the cycling performance of NMC622//Cu at a current density of 0.5–2 mA cm^{-2} and voltage range of 2.5–4.2 V. The comparison of cycling at 0.5 mA cm^{-2} was depicted in Fig. S4a, which shows the control cells underwent quickly degraded capacity even at the initial cycle while the magnetic cells demonstrate extended to 16 cycles. Figs. S4b–4c describes the discharge capacity and Coulombic efficiency for these two group cells. Both delivered capacities in the magnetic group are superior to the control ones. A similar phenomenon was also observed at the higher current density of 2 mA cm^{-2} in Figs. S4d–4e It is worth noting that the magnetic control demonstrates extended cycling behaviours. However, the cycling performance is still poor, and the capacity degraded quickly in anode-free lithium metal cells for the

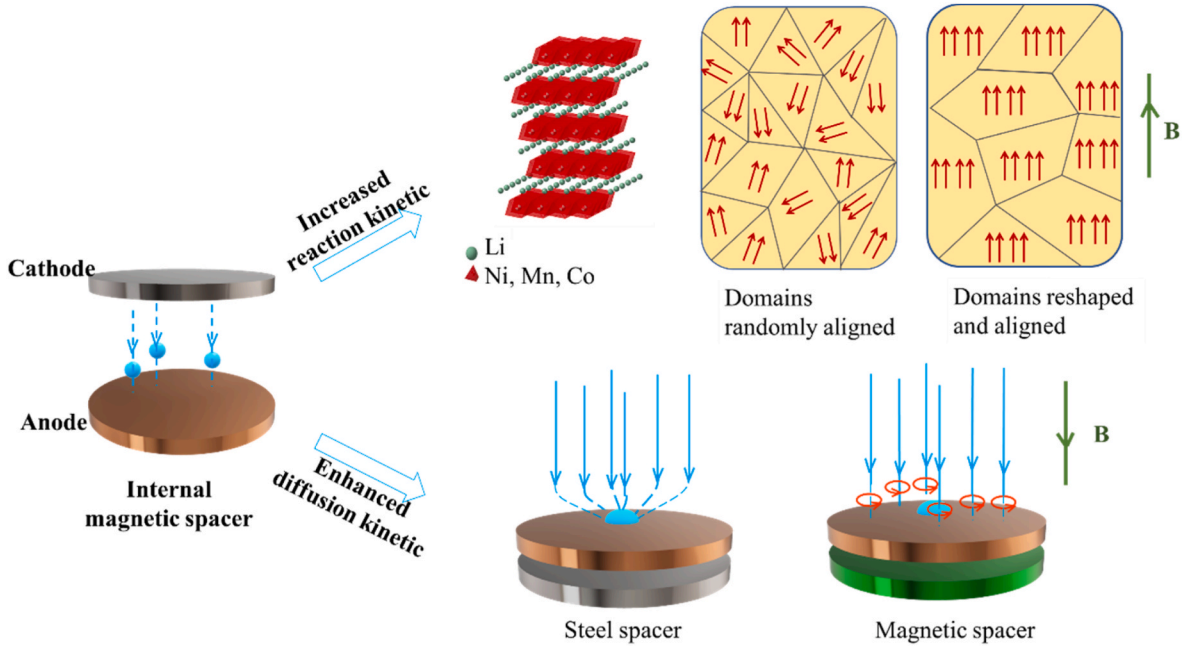

Fig. 1. Schematic illustration of magnetic effect on dependent cathode and anode of full cells: (1) Increased reaction kinetic at the ferromagnetic cathode: the input and non-contact magnetic energy transfer the ferromagnetic Ni from randomly aligned domains to reshaped domains, thus generating more unpaired electrons and increase the reaction kinetic at the cathode); (2) Diffusion enhancements (red circles) along the anode surface due to the MHD effect on moving Li^+/Na^+. (For interpretation of the references to colour in this figure legend, the reader is referred to the Web version of this article.)

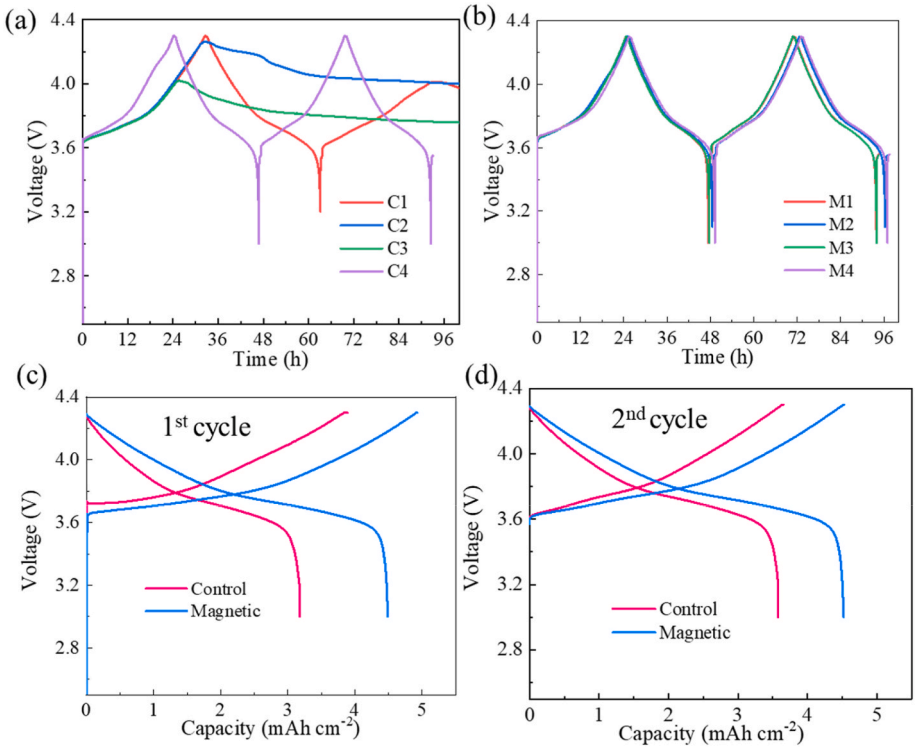

Fig. 2. Voltage vs time evolution in formation cycles for the control group (a) and magnetic group (b). The voltage and overpotential of 1st (c) and 2nd (d) cycle for control and magnetic group.

magnetic group. This is due to the poor connection between the deposited lithium and the current collector, which would increase the contact resistance of lithium-free NMC622//Cu cell and result in a fast capacity loss. SEM characterizations were performed to examine the morphology evolution at the anode-free lithium metal electrode (current collector). Fig. 3 compared the deposited lithium morphology for the control and magnetic groups after cycling at the current density of 2 mA cm^{-2}. The loosely deposited dendritic structures are proliferated at the current collectors in Fig. 3a–b while the dense deposited lithium morphology dominated at the anode surface, thus achieving the dendrite-free morphology, and stabilizing the lithium-free anode in Fig. 3c–d.

The methodology was extended to the sodium-ion battery. After the formation cycles (C/20 × 2), the C/5 rate was used to charge the cell up to 4.2 V. Following this, the cells were disassembled to investigate the deposited morphology of Na^+ at the anode-free sodium metal (Al current collector). Fig. 3e–f demonstrates the large amounts of sodium dendritic structures with a maximal length of 30 μm at the current collector. Fig. S5 shows the separator side which faces the current collector. The yellow marks on the separator confirmed the sparsely island-distributed deposited sodium. This poses a high possibility of piercing the separator, inducing the safety issue, and degrading cell capacity. By comparison, the dendrite-free morphology was observed, and the dense particle largely conquered the Al current collector (Fig. 3g–h). On this regard, the dendrite-free morphology would reduce the safety issues and lower the overpotential of the cell to contribute to the extended cell performance.

3.3. Enhancement of electrode kinetics

Fast diffusion reaction kinetics usually lead to high-rate cell performance. These two kinetic parameters are reflected in the overpotential of cells and can be extrapolated from the cell voltage and the delivered cell capacities. To reveal the magnetic effect on each independent electrode of the cell, GITT, and EIS techniques were adopted to quantify the diffusion and reaction kinetics of the electrode. The anode-free lithium metal cell (NMC622//Cu) and full coin cells (NMC622//graphite) with an area capacity of 4 mA h cm^{-2} were evaluated.

For the GITT pulse, a 10-min charge/discharge followed by a 2-h open-circuit voltage (OCV) period was conducted to achieve full equilibrium. Additionally, EIS tests were performed at different state-of-charges (SoCs) including 25 %, 50 %, 75 %, and 100 %. An example of EIS for full NMC622//graphite electrodes is shown in Fig. S6a. By combining GITT and EIS measurements at every 20% SoC throughout the charge/discharge capacity, the diffusion and reaction kinetics of both the control and magnetic groups were achieved, as presented in Fig. 4. Fig. 4a displays the GITT profiles at C/10 and OCV (2 h) for the two groups on NMC622//Cu cells. Initially, the voltage of both groups is nearly the same during charging. However, as the charge continues, the voltage starts to diverge between the control and magnetic groups. The magnetic group exhibits lower overpotential compared to the control group and eventually achieves higher charge capacities. A similar trend is observed during the discharge process. Next, the diffusion kinetics of NMC622//Cu is depicted in Fig. 4b. Throughout the entire charge and discharge process, the diffusion in NMC622//Cu shows little difference. This is expected because NMC622 with high mass loading of 4 mA h cm^{-2} is not the diffusion-limiting electrode in the cells. Therefore, it is challenging to improve the diffusion kinetics of Li^+ in the porous electrode. However, the internal magnetic field enhances the reaction kinetics of cells by reducing the charge-transfer resistance (Rct) of the ferromagnetic NMC622 cathode, as shown in Fig. 4c. The detailed equivalent circuit has been shown in Fig. S6b. This enhanced reaction kinetics in NMC622 could be attributed to an alignment of the ferromagnetic domains in the crystallites. It is observed however that the kinetics are improved even at 100% state of charge in magnetic group, where the material is mostly paramagnetic (Ni^{4+}). However, the relative decrease in R_{ct} between the 75 and 100% state of charge reduces compared to the sample with no applied magnetic field, as shown in Fig. 4c. On top of this, a similar reduction in Rct by the internal magnetic field is also observed at higher C rates of C/5, as seen in Fig. S7.

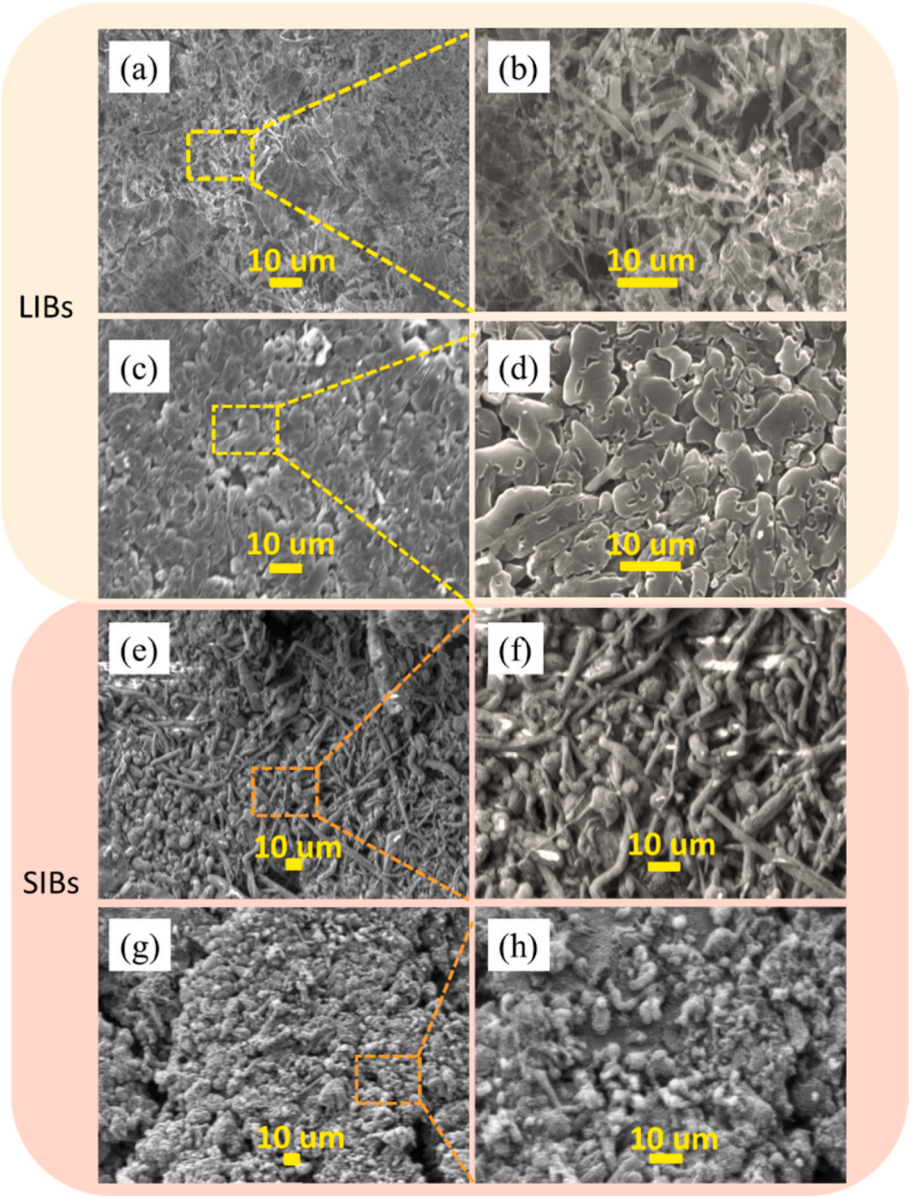

Fig. 3. Comparison of deposited morphology between control and magnetic group by SEM characterizations: the morphology evolution of control case ((a)–(b)) and magnetic case ((c)–(d)) for LIB after cycling at the current density of 2 mA cm^{-2}. The morphology evolution of control case ((e)–(f)) and magnetic case ((g)–(h)) for SIB at 4.2 V. The scale bars are 10 μm.

To further investigate the magnetic effect on the graphite anode, the investigation was extended to full cells using the NMC622//graphite chemistry. Fig. 4d presents the voltage behaviour during GITT measurements for the full coin cells. Similar to the findings in the magnetic half cells, the full cells with the internal magnetic field also exhibited lower overpotential and higher capacity throughout the pulse charge/discharge process. Additionally, the diffusion kinetics at the porous and thickening negative electrode (graphite) was improved in Fig. 4e. This diffusion enhancement could be attributed to the fact that graphite, with its high mass loading, acts as the diffusion-limiting electrode in the full-cell configuration [37]. The magnetohydrodynamic (MHD) effect can enhance diffusion within this diffusion-limiting graphite anode. Regarding the reaction kinetics, the charge-transfer resistance (Rct) was also reduced when the internal magnetic field was applied (Fig. 4f). As expected, both the diffusion and reaction kinetics of the full cells were found to be influenced by the internal magnetic field in the full-cell configuration. These results confirm the magnetic effect on enhancing the reaction kinetics at the ferromagnetic cathode and the diffusion kinetic at the rate-limiting porous graphite anode.

3.4. Magnetic effects on cell cycling performance

To examine the effect of the internal magnetic field on cycling performance, full commercial coin cells with the NMC622//graphite chemistry and area capacities of 4 mA h cm^{-2} were evaluated at current densities of 0.5 and 2 mA cm^{-2}. Fig. 5a–b illustrates the cycling performance of the NMC622//graphite full coin cells at a current density of 0.5 mA cm^{-2}. For the cell tests, the cell voltage ranged from 2.5 to 4.2 V for 200 cycles.

At the initial cycles, both the control group (represented by red scatter and error band from 5 coin cells) and the magnetic group (represented by blue scatter and error band from 5 coin cells) exhibit almost the same discharge capacities, with a value of 4.08 mA h cm^{-2}. However, as cycling continues, the discharge capacity of the control group (red scatter and error band) drops much faster compared to the magnetic group (blue scatter). In Fig. 4a, it can be observed that the discharge

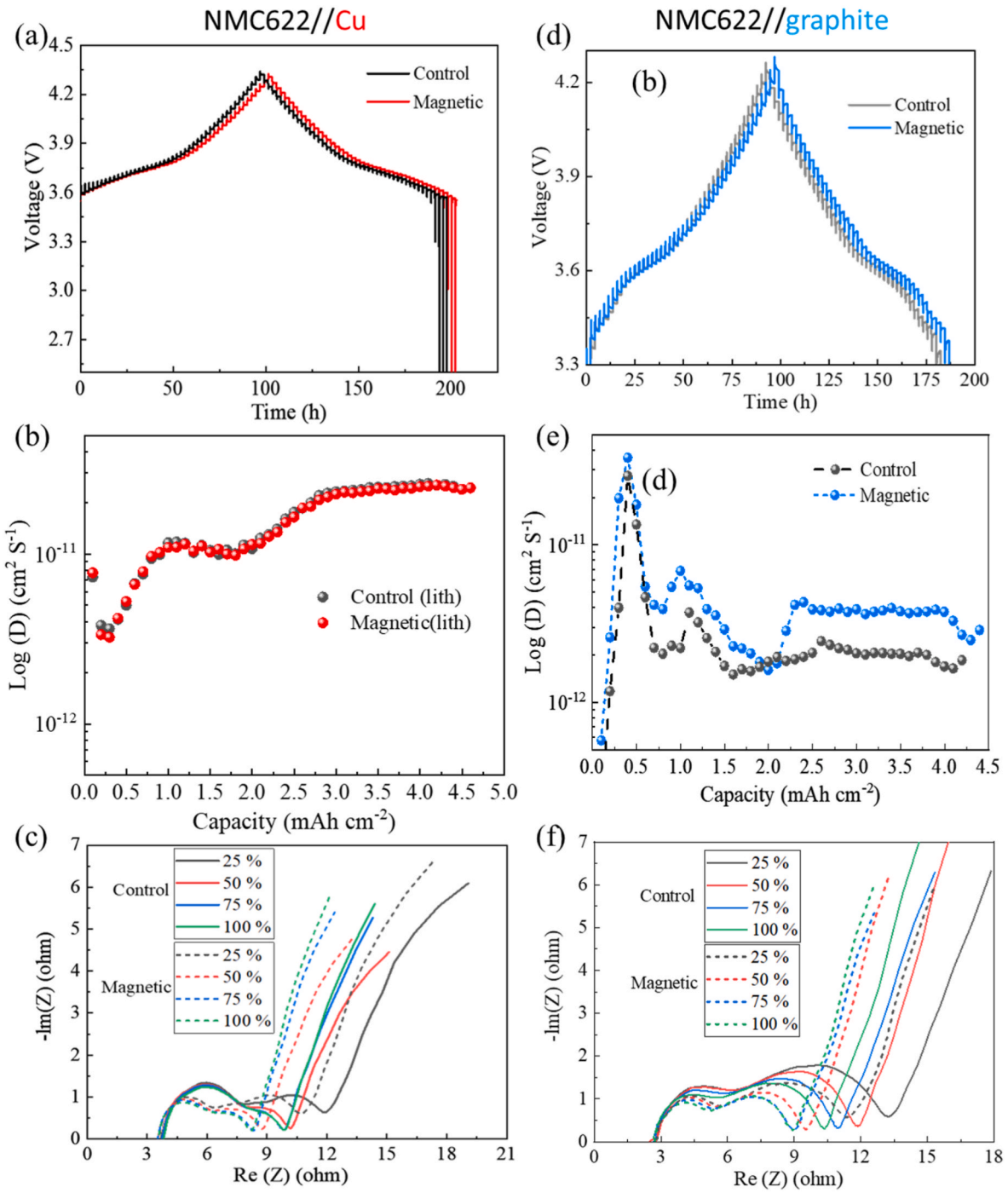

Fig. 4. Revealing the electrode kinetic of cells at C/10 for NMC622//Cu (a–c) and NMC622//graphite (*d*–f) with/without the magnetic field: GITT profiles(a), diffusion kinetic(b), and EIS tests at varying SoCs (c) for NMC622//Cu; GITT profiles(d), diffusion kinetic(e), and EIS tests (f) at varying SoCs for NMC622//graphite.

capacity of the control group decreases to 2.8 mA h cm^{-2} after 200 cycles, whereas the magnetic group maintains a capacity of 3.75 mA h cm^{-2}, indicating better capacity retention. In terms of Coulombic efficiency (CE), the magnetic group demonstrates noticeably higher values compared to the control group. It is worth noting that the CEs of the control group varied widely, ranging from 70% to 98%. However, the CEs of the magnetic group remained stable at 98% throughout the entire cycling process. This indicates enhanced diffusion and reaction kinetics of the electrode in the full cells with a capacity of 4 mA h cm^{-2}, as well as the stabilization of the graphite anode by mitigating dendritic issues at a current density of 0.5 mA cm^{-2} during cell cycling.

With the increasing current density to 2 mA cm^{-2} in Fig. 2c–d, both the control case and magnetic groups present a slight decrease in initially delivered capacities to 3.75 mA h cm^{-2}. This decrease is expected as thicker electrodes tend to exhibit degraded capacities due to limited kinetics, especially at higher current densities. However, the control case shows a more rapid decrease in discharge capacities compared to the magnetic group. At the end of the cycles, the discharge capacities for the control and magnetic groups are 2.55 and 3.45 mA h cm^{-2}, respectively. The error bands representing cell-to-cell performance are much smaller for the magnetic group, indicating superior cell stability. This superior stability of the magnetic group is further supported by the Coulombic efficiency (CE) shown in Fig. 4d. The CEs of the magnetic group are higher than those of the control group, and the

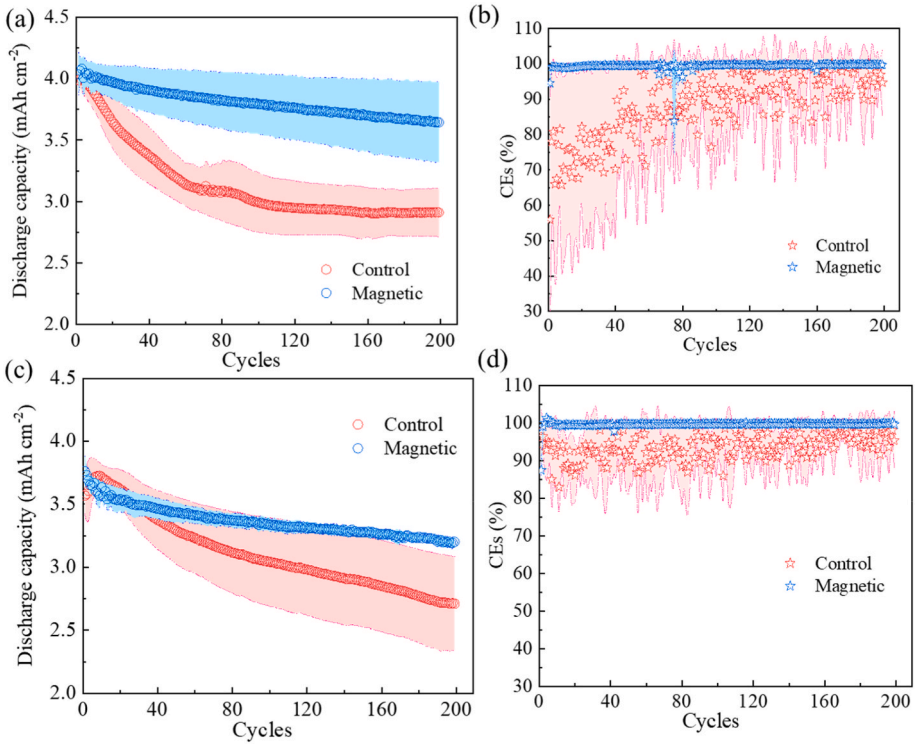

Fig. 5. Cycling performance with/without the magnetic field for NMC622//graphite: (a) discharge capacities retention and CEs (b) of two groups at the current density of 0.5 mA cm^{-2}. (c) Discharge capacities retention and CEs (d) of two groups at the current density of 2 mA cm^{-2}.

variation in discharge capacity is negligible. The methodology was also extended to sodium-ion batteries (NMST//HC) in Fig. S8, where cycling at C/5 charge and discharge for up to 50 cycles was performed. The results also demonstrate enhanced cell performance due to the presence of the internal magnetic spacer. Therefore, both the full lithium-ion batteries (NMC622//graphite) and sodium-ion batteries (NMST//HC) coin cells exhibited improved electrochemical behaviour and enhanced electrode kinetics and stability in the presence of the internal magnetic field.

Table 1 summarizes a comparison of different lithium-ion battery exposed to a magnetic field. The magnet position, cell chemistry, areal capacity, current density, magnetic field strength, and cycle performance are compared. In this work, an internal rare earth magnet was incorporated into the cell with a constant magnetic field strength, high coat weights (4 mA h cm^{-2}) in a full cell, and several novel cell chemistries; sodium -ion, zero excess lithium and sodium, also show improvements in reproducibility and cycle life when formed and cycled in a magnetic field.

The improvements in formation, rate, reproducibility, and cycle life due to improved ionic diffusivity, electron kinetics at the positive electrode and metal plating morphology for several different cell chemistries indicate that performance improvements would also be observed for other battery chemistries would be observed with an applied magnetic field. This includes electrochemical cells which strip and plate metals in aqueous or non-aqueous ionically conducting electrolytes. Examples include metal-ion, metal-air batteries or metal anodes with various electrochemical system (i.e., Li, Na, K, Ca, etc.)

4. Conclusion

The application of an internal magnetic field generated by a hard magnetic spacer (NdFeB) is applied to several cell chemistries such as lithium and sodium-ion, zero excess lithium and sodium metal and in all cases, improvements in reproducibility in achieved capacity, rate and cycle-life is observed.

For the cell formation at low C rates, the internal magnetic field stabilizes the anode-free lithium/sodium metal by achieving a uniform distribution of Li^+/Na^+ at the current collector. This enhanced mass transport both on the anode-free lithium/sodium metal and the porous active material of the anode, resulting in reduced full cell overpotential. As a high charge and discharge capacity for a high energy full cell is observed. Electrochemical impedance spectroscopy (EIS) and

Table 1
The comparison between magnetic spacer and previous work.

Magnet	Cell chemistry	Capacity/mAh cm^{-2}	Current/mA cm^{-2}	Strength/mT	Cycle number	Data
Outside the cell	NMC532//Li	0.5	1	400	100	Ref [39]
		0.5	4		~400	
		1	0.5		360	
	LFP//Li	0.5	1	350	200	Ref [27]
		1	2		120	
	Li//Li@Cu	0.5	0.25	0.6	180	Ref [28]
		1	1	0.6	120	
	LCO//Li	1	1	160	650	Ref [40]
	Li//Li@Cu	1	2	800	2603	Ref [26]
Magnetic spacer	NMC622//graphite	4	0.5	35	200	Manuscript
			2		200	

galvanostatic intermittent titration technique (GITT) investigations on anode-free lithium metal cells and full cells provide insights into the magnetic effect on individual electrodes. Faster reaction kinetics are observed at the ferromagnetic cathode, likely due to the alignment of the spins on the nickel. On the negative electrode, the MHD effect generated by the internal magnetic further homogenizes the Li^+ ion flux for both the anode-free metal and the thick, porous electrode. In addition, through the introduction of an internal magnetic field, the cycling performances of the full lithium-ion batteries (NMC622//graphite) and sodium-ion batteries (NMST//HC) were extended and improved.

This work illustrates the benefits of applying a magnetic field to a battery and shows the improvement in formation reproducibility and the enhancement in observed capacity, rate, and cycle life for several different cell chemistries. This improvement is due to the improved ionic diffusivity, enhanced surface kinetics, and plating morphology of the metal at the negative electrode, suggesting a benefit would also be observed for other novel cell chemistries which are developed in the future.

CRediT authorship contribution statement

Yongxiu Chen: Writing – original draft, Methodology, Investigation, Data curation, Conceptualization. **James Alder:** Writing – review & editing, Investigation. **Tengfei Song:** Writing – review & editing, Investigation. **Lin Chen:** Writing – review & editing, Investigation. **Richard Sheridan:** Writing – review & editing, Investigation. **Alison Davenport:** Writing – review & editing, Investigation. **Emma Kendrick:** Writing – review & editing, Supervision, Project administration, Methodology, Funding acquisition, Conceptualization.

Declaration of competing interest

The authors declare that they have no known competing financial interests or personal relationships that could have appeared to influence the work reported in this paper.

Data availability

Data will be made available on request.

Acknowledgements

We acknowledge the funding support received from the Faraday Institution (grant number FIRG059).

Appendix A. Supplementary data

Supplementary data to this article can be found online at https://doi.org/10.1016/j.jpowsour.2024.234323.

References

[1] Y. Xu, D. Bauer, M. Lübke, T.E. Ashton, Y. Zong, J.A. Darr, High-power sodium titanate anodes; a comparison of lithium vs sodium-ion batteries, J. Power Sources 408 (2018) 28–37, https://doi.org/10.1016/j.jpowsour.2018.10.038.

[2] P. Yang, Y. Cao, X. Zhang, Y. Xie, Y. Cui, S. Ma, K. Wei, Y. Wei, C. Wang, X. Li, Electrochemical behaviors in low-cost and environmentally stable SnS_2: an alternative cathode with for high-power primary lithium batteries, J. Power Sources 541 (2022), https://doi.org/10.1016/j.jpowsour.2022.231717.

[3] Y. Ye, L.-Y. Chou, Y. Liu, H. Wang, H.K. Lee, W. Huang, J. Wan, K. Liu, G. Zhou, Y. Yang, A. Yang, X. Xiao, X. Gao, D.T. Boyle, H. Chen, W. Zhang, S.C. Kim, Y. Cui, Ultralight and fire-extinguishing current collectors for high-energy and high-safety lithium-ion batteries, Nat. Energy 5 (10) (2020) 786–793, https://doi.org/10.1038/s41560-020-00702-8.

[4] D.Y. Yu, P.V. Prikhodchenko, C.W. Mason, S.K. Batabyal, J. Gun, S. Sladkevich, A. G. Medvedev, O. Lev, High-capacity antimony sulphide nanoparticle-decorated graphene composite as anode for sodium-ion batteries, Nat. Commun. 4 (2013) 2922, https://doi.org/10.1038/ncomms3922.

[5] F. Cheng, H. Wang, Z. Zhu, Y. Wang, T. Zhang, Z. Tao, J. Chen, Porous $LiMn_2O_4$ nanorods with durable high-rate capability for rechargeable Li-ion batteries, Energy Environ. Sci. 4 (9) (2011), https://doi.org/10.1039/c1ee01795k.

[6] Kisuk Kang, Ying Shirley Meng, Julien Breger, Clare P. Grey, G. Ceder, Electrodes with high power and high capacity for rechargeable lithium batteries, Science 311 (5763) (2006) 977–980, https://doi.org/10.1126/science.1122152.

[7] S. Lou, X. Cheng, Y. Zhao, A. Lushington, J. Gao, Q. Li, P. Zuo, B. Wang, Y. Gao, Y. Ma, C. Du, G. Yin, X. Sun, Superior performance of ordered macroporous $TiNb_2O_7$ anodes for lithium ion batteries: understanding from the structural and pseudocapacitive insights on achieving high rate capability, Nano Energy 34 (2017) 15–25, https://doi.org/10.1016/j.nanoen.2017.01.058.

[8] P.L. Taberna, S. Mitra, P. Poizot, P. Simon, J.M. Tarascon, High rate capabilities Fe_3O_4-based Cu nano-architectured electrodes for lithium-ion battery applications, Nat. Mater. 5 (7) (2006) 567–573, https://doi.org/10.1038/nmat1672.

[9] Z. Li, K. Zhu, P. Liu, L. Jiao, 3D confinement strategy for dendrite-free sodium metal batteries, Adv. Energy Mater. 12 (4) (2021), https://doi.org/10.1002/aenm.202100359.

[10] Shu-Lei Chou, Jia-Zhao Wang, Jia-Zeng Sun, David Wexler, Maria Forsyth, Hua-Kun Liu, Douglas R. MacFarlane, S.-X. Dou, High capacity, safety, and enhanced cyclability of lithium metal battery using a V_2O_5 nanomaterial cathode and room temperature ionic liquid electrolyte, Chem. Mater. 20 (2008) 7044–7051, https://doi.org/10.1021/cm801468q.

[11] D. Wang, C. Qin, X. Li, G. Song, Y. Liu, M. Cao, L. Huang, Y. Wu, Synchronous healing of Li metal anode via asymmetrical bidirectional current, iScience 23 (1) (2020) 100781, https://doi.org/10.1016/j.isci.2019.100781.

[12] N. Balke, S. Jesse, A.N. Morozovska, E. Eliseev, D.W. Chung, Y. Kim, L. Adamczyk, R.E. Garcia, N. Dudney, S.V. Kalinin, Nanoscale mapping of ion diffusion in a lithium-ion battery cathode, Nat. Nanotechnol. 5 (10) (2010) 749–754, https://doi.org/10.1038/nnano.2010.174.

[13] J.S. Edge, S. O'Kane, R. Prosser, N.D. Kirkaldy, A.N. Patel, A. Hales, A. Ghosh, W. Ai, J. Chen, J. Yang, S. Li, M.C. Pang, L. Bravo Diaz, A. Tomaszewska, M. W. Marzook, K.N. Radhakrishnan, H. Wang, Y. Patel, B. Wu, G.J. Offer, Lithium ion battery degradation: what you need to know, Phys. Chem. Chem. Phys. 23 (14) (2021) 8200–8221, https://doi.org/10.1039/d1cp00359c.

[14] Q. Wang, H. Yang, T. Meng, J. Yang, B. Huang, F.L. Gu, S. Zhang, C. Meng, Y. Tong, Boosting electron transfer with heterointerface effect for high-performance lithium-ion storage, Energy Storage Mater. 36 (2021) 365–375, https://doi.org/10.1016/j.ensm.2021.01.003.

[15] Y. Chen, H. Huang, L. Liu, Y. Chen, Y. Han, Diffusion enhancement to stabilize solid electrolyte interphase, Adv. Energy Mater. 11 (40) (2021), https://doi.org/10.1002/aenm.202101774.

[16] Z. Ju, J. Nai, Y. Wang, T. Liu, J. Zheng, H. Yuan, O. Sheng, C. Jin, W. Zhang, Z. Jin, H. Tian, Y. Liu, X. Tao, Biomacromolecules enabled dendrite-free lithium metal battery and its origin revealed by cryo-electron microscopy, Nat. Commun. 11 (1) (2020) 488, https://doi.org/10.1038/s41467-020-14358-1.

[17] X. Sun, X. Zhang, Q. Ma, X. Guan, W. Wang, J. Luo, Revisiting the electroplating process for lithium-metal anodes for lithium-metal batteries, Angew Chem. Int. Ed. Engl. 59 (17) (2020) 6665–6674, https://doi.org/10.1002/anie.201912217.

[18] D. Wang, T. Xie, C. Qin, X. Wang, G. Li, Y. Liu, H. Zou, L. Huang, Y. Wu, Artificial sei film via synchronous reaction-diffusion-assembly on Li liquid metal, Adv. Funct. Mater. 32 (48) (2022), https://doi.org/10.1002/adfm.202206405.

[19] T.-S. Wang, Y. Liu, Y.-X. Lu, Y.-S. Hu, L.-Z. Fan, Dendrite-free Na metal plating/stripping onto 3d porous cu hosts, Energy Storage Mater. 15 (2018) 274–281, https://doi.org/10.1016/j.ensm.2018.05.016.

[20] S.S. Zhang, A review on electrolyte additives for lithium-ion batteries, J. Power Sources 162 (2) (2006) 1379–1394, https://doi.org/10.1016/j.jpowsour.2006.07.074.

[21] M. Wang, J. Wang, J. Si, F. Chen, K. Cao, C. Chen, Bifunctional composite separator with redistributor and anion absorber for dendrites-free and fast-charging lithium metal batteries, Chem. Eng. J. 430 (2022), https://doi.org/10.1016/j.cej.2021.132971.

[22] J.Y. Song, Y.Y. Wang, C.C. Wan, Review of gel-type polymer electrolytes for lithium-ion batteries, J. Power Sources 77 (1999) 183–197, https://doi.org/10.1016/S0378-7753(98)00193-1.

[23] Li Qi, Shen Tan, Linlin Li, Yingying Lu, Y. He, Understanding the molecular mechanism of pulse current charging for stable lithium-metal batteries, Sci. Adv. 3 (2017) e1701246, https://doi.org/10.1126/sciadv.1701246.

[24] Z. Zhang, Z.L. Wang, X. Lu, Suppressing lithium dendrite growth via sinusoidal ripple current produced by triboelectric nanogenerators, Adv. Energy Mater. 9 (20) (2019), https://doi.org/10.1002/aenm.201900487.

[25] Y. Chen, X. Dou, K. Wang, Y. Han, Lithium dendrites inhibition via diffusion enhancement, Adv. Energy Mater. 9 (17) (2019), https://doi.org/10.1002/aenm.201900019.

[26] Y. Chen, X. Dou, K. Wang, Y. Han, Magnetically enhancing diffusion for dendrite-free and long-term stable lithium metal anodes, Green Energy Environ. 7 (5) (2022) 965–974, https://doi.org/10.1016/j.gee.2020.12.014.

[27] K. Shen, Z. Wang, X. Bi, Y. Ying, D. Zhang, C. Jin, G. Hou, H. Cao, L. Wu, G. Zheng, Y. Tang, X. Tao, J. Lu, Magnetic field–suppressed lithium dendrite growth for stable lithium-metal batteries, Adv. Energy Mater. 9 (20) (2019), https://doi.org/10.1002/aenm.201900260.

[28] A. Wang, Q. Deng, L. Deng, X. Guan, J. Luo, Eliminating tip dendrite growth by lorentz force for stable lithium metal anodes, Adv. Funct. Mater. 29 (25) (2019), https://doi.org/10.1002/adfm.201902630.

[29] Q. Li, S. Zhu, Y. Lu, 3D porous cu current collector/li-metal composite anode for stable lithium-metal batteries, Adv. Funct. Mater. 27 (18) (2017), https://doi.org/10.1002/adfm.201606422.

[30] R. Zhang, N.W. Li, X.B. Cheng, Y.X. Yin, Q. Zhang, Y.G. Guo, Advanced micro/nanostructures for lithium metal anodes, Adv. Sci. 4 (3) (2017) 1600445, https://doi.org/10.1002/advs.201600445.
[31] J. Qian, W. Xu, P. Bhattacharya, M. Engelhard, W.A. Henderson, Y. Zhang, J.-G. Zhang, Dendrite-free Li deposition using trace-amounts of water as an electrolyte additive, Nano Energy 15 (2015) 135–144, https://doi.org/10.1016/j.nanoen.2015.04.009.
[32] J. Shim, D.G. Kim, H.J. Kim, J.H. Lee, J.C. Lee, Polymer composite electrolytes having core-shell silica fillers with anion-trapping boron moiety in the shell layer for all-solid-state lithium-ion batteries, ACS Appl. Mater. Interfaces 7 (14) (2015) 7690–7701, https://doi.org/10.1021/acsami.5b00618.
[33] B. Kishore, L. Chen, C.E.J. Dancer, E. Kendrick, Electrochemical formation protocols for maximising the life-time of a sodium ion battery, Chem. Commun. 56 (85) (2020) 12925–12928, https://doi.org/10.1039/d0cc05673a.
[34] I. Rubio Lopez, M.J. Lain, E. Kendrick, Optimisation of formation and conditioning protocols for lithium-ion electric vehicle batteries, Batter. Supercaps 3 (9) (2020) 900–909, https://doi.org/10.1002/batt.202000048.
[35] A. Bund, S. Koehler, H.H. Kuehnlein, W. Plieth, Magnetic field effects in electrochemical reactions, Electrochim. Acta 49 (1) (2003) 147–152, https://doi.org/10.1016/j.electacta.2003.04.009.
[36] L.M.A. Monzon, J.M.D. Coey, Magnetic fields in electrochemistry: the lorentz force. A mini-review, Electrochem. Commun. 42 (2014) 38–41, https://doi.org/10.1016/j.elecom.2014.02.006.
[37] Y. Chen, J. Key, K. O'Regan, T. Song, Y. Han, E. Kendrick, Revealing the rate-limiting electrode of lithium batteries at high rates and mass loadings, Chem. Eng. J. 450 (2022), https://doi.org/10.1016/j.cej.2022.138275.
[38] Y. Hui, Y. Wu, W. Sun, X. Sun, G. Huang, Z. Na, Nanosecond pulsed laser-assisted deposition to construct a 3d quasi-gradient lithiophilic skeleton for stable lithium metal anodes, Adv. Funct. Mater. (2023) 2303319, https://doi.org/10.1002/adfm.202303319.
[39] J. Dong, H. Dai, C. Wang, C. Lai, Uniform lithium deposition driven by vertical magnetic field for stable lithium anodes, Solid State Ion. (2019) 341, https://doi.org/10.1016/j.ssi.2019.115033.
[40] Huang, X. Wu, L. Nie, S. Chen, Z. Sun, Y. He, W. Liu, Mechanism of lithium electrodeposition in a magnetic field, Solid State Ion. 345 (2020), https://doi.org/10.1016/j.ssi.2019.115171.